Resonances and critical points in the strong-field ionization of diatomic molecules

George N. Gibson,* Hui Chen, and Dale L. Smith
Department of Physics, University of Connecticut, Storrs, Connecticut 06269, USA

(Received 20 May 2019; published 19 August 2019)

We measured the strong-field ionization of diatomic iodine molecules as a function of wavelength and internuclear separation. The latter was done by launching a wave packet on the B state of iodine and probing the ionization as a function of time delay. As a function of wavelength at fixed internuclear separation and as a function time delay at fixed wavelength, critical points are found where the ionization increases significantly. All of the results are consistent with ionization from deep σ orbitals and resonant interactions. In conclusion, we present a unified view of the strong-field ionization of diatomic molecules.

DOI: 10.1103/PhysRevA.100.023412

I. INTRODUCTION

While the behavior of atoms in strong fields is relatively well understood, even simple molecules exhibit a far richer range of phenomena, including enhanced ionization at a critical internuclear separation R_c [1,2], vibrational [3,4] and electronic [5,6] excitation, inner-orbital ionization [7], and high-harmonic generation [8]. The last has opened a new field of high-harmonic molecular spectroscopy [9]. All of these strong-field effects start with single-electron ionization, highlighting the need to understand this primary event, in detail.

The simplest class of molecules, homonuclear diatomics, themselves deviate significantly from atoms, when exposed to strong laser fields. Standard tunneling models predict that the least bound electron will account for virtually all of the single-electron ionization and the resulting ion will then be left in the ground state [10]. Some population is left in Rydberg states, through multiphoton excitation [11] or frustrated tunneling ionization [12], but the amount is relatively small [6]. Diatomic molecules, however, show a high degree of excitation. The earliest and simplest manifestation of this is the observation that evenly charged molecular ions often dissociate into charge-asymmetric fragments, for example, $N_2{}^{4+} \rightarrow N^{3+} + N^{1+}$. The molecular potential curves that can access these charge-asymmetric dissociation limits lie quite high in energy [13].

Besides charge-asymmetric dissociation, the excitation of molecules by strong laser fields can be seen directly by observing prompt vacuum-ultraviolet (VUV) radiation following strong-field ionization [6]. VUV spectroscopy reveals the upper and lower states of a transition, and we have seen states 30 eV above the ground state radiating, following ionization by 800 nm radiation. This represents a transition of 20 photons to a bound excited state. For the most part, the prompt (nonplasma) radiation comes from atomic ions following dissociation, and all of the excited states seen to radiate consisted of one or two holes in the outer most s shell, suggesting direct ionization of inner σ orbitals built on the s subshell electrons. In our experiments, no such radiation was seen from argon atoms. Thus, while excitation of Rydberg states undoubtedly occurs, the degree of excitation through this mechanism is much less than through ionization of inner-orbital electrons, at least in molecules.

Diatomic molecules also show interesting behavior as a function of internuclear separation R. It has been seen experimentally and well understood theoretically that the ionization rate peaks at a critical separation R_c and then falls off to atomic-like rates at large R [1,2]. Moreover, it has been predicted to occur for σ orbitals, but not the higher angular momentum orbitals, such as π or δ orbitals [14].

Tunneling ionization is only weakly dependent on wavelength in the optical frequency range, but it has been observed that there are critical points in the wavelength dependence of the ionization of iodine [15]. Around the X to B state resonance, the ionization changes dramatically over a very small range of wavelengths [16]. Just above the resonance, at 519 nm, the branching ratio of ionization from inner orbitals reaches a peak of 98%, while at 580 nm the branching ratio reaches a minimum of 88%. In either case, it is remarkable that the branching ratio for inner orbital ionization is so high. The X to B state transition moves population from the HOMO (highest occupied molecular orbital) to LUMO (lowest unoccupied molecular orbital), where one might expect rapid ionization of the LUMO, leaving the molecular ion in the X ground state. However, this is not what is observed.

Iodine is a particularly instructive molecule, as its ground-state vibrational period is 155 fs, while the period of the B state is around 750 fs, depending on the exact wavelength used to populate the B state [17]. In either case, the motion of the iodine atoms can be fully resolved in time, and, hence, R. In addition, there are various inner orbitals that can be accessed by the strong laser field [17]. The electronic orbitals of I_2 are

$$[\text{core}]^{92}10\sigma_g^2 10\sigma_u^2 11\sigma_g^2 6\pi_u^4 6\pi_g^4 11\sigma_u^0. \quad (1)$$

We define ionization from the $11\sigma_g$, $6\pi_u$, $6\pi_g$ orbitals as outer-orbital ionization (OOI) and ionization from the $10\sigma_u$, $10\sigma_g$ orbitals as inner-orbital ionization (IOI) [15]. We also refer to the orbitals as follows: $6\pi_g$ (HOMO), $6\pi_u$ (HOMO-1), $11\sigma_g$ (HOMO-2), $10\sigma_u$ (HOMO-3), and $10\sigma_g$ (HOMO-4).

*george.gibson@uconn.edu

In this paper, we present experimental results from pump-probe measurements. As a function of time delay, numerous distinct critical points are found in the ionization rate to different final states, corresponding to the ionization of different inner orbitals. In particular, we monitor signals from I_2^+, energy-resolved $I^+ + I\,(1, 0)$, $I^+ + I^+\,(1, 1)$, $I^{2+} + I\,(2, 0)$, and $I^{2+} + I^+\,(2, 1)$. Previously we showed that critical points occur as a function of wavelength at fixed R (the equilibrium value R_{eq}). We now show that they occur as a function of R, at fixed wavelength. In addition, single-photon resonances appear to play an important role in coupling to the inner orbitals.

II. EXPERIMENT

We use a Spitfire (Spectra Physics) ultrashort pulse laser system, which produces 35 fs, 800 nm laser pulses at 1 kHz. Part of the laser is used to pump a TOPAS (Light Conversion) optical parametric amplifier, which can generate ~10 μJ of energy at 513 nm in a 40 fs pulse, measured with an achromatic third-order autocorrelator. The remaining 800 nm radiation is delayed in time with a computer-controlled translation stage to perform the pump-probe measurements. The polarization of both beams is linear and parallel to each other. The ions resulting from the strong-field interaction are measured in a spectrometer with a microchannel plate detector. We used both time-of-flight (TOF) and velocity map imaging (VMI) modes. For the TOF experiments, the laser polarization is along the TOF axis, while for VMI, it is perpendicular. Iodine is introduced effusively into the detection chamber, which has a base pressure in the range of 10^{-9} torr, while the iodine pressure is kept around 2×10^{-7} torr.

We simulate the time evolution of the wave packet placed on the B state by the pump pulse. From these simulations, we can determine the expectation value $\langle R \rangle$ as a function of time (see Fig. 1). However, this can be misleading, as the wave packet evolution is rather complicated. So we also calculate the width of the wave packet (also in Fig. 1). Finally, to understand certain features in the data, we must consider the entire shape of the wave packet, shown in Fig. 2. We focus primarily on the TOF data, as they have higher energy resolution. The VMI data were used to confirm the TOF results and to check for critical points in molecules whose molecular axis lies perpendicular to the polarization axis of the laser. While the VMI data reproduced the TOF results for molecules parallel to the polarization axis, no critical points were found in other directions.

III. RESULTS

Figure 3 shows the complete TOF data set for I_2^+, I^+, and I^{2+}. The x axis is TOF. As can be seen, the TOF spectrometer is configured for symmetric energy dispersion, where the energy comes from the kinetic energy release (KER) following dissociation. The y axis is pump-probe delay. Zero-time delay is not shown due to the large, but unimportant, increase in signal when the pump and probe overlap in time. As can be seen, there are several critical points where the ionization peaks for various different channels. Interestingly, the peaks generally occur at different times, corresponding to different internuclear separations. We now consider each channel separately.

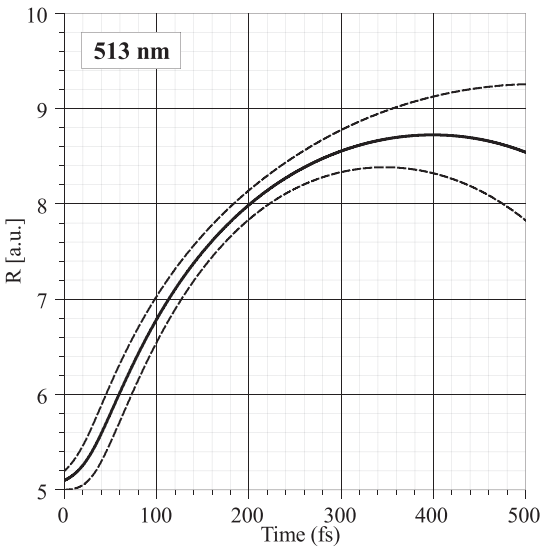

FIG. 1. Simulation of the time evolution of the vibrational wave packet excited from the X to the B state with 513 nm radiation. Solid line corresponds to $\langle R \rangle$; dashed lines correspond to the rms width of the wave packet.

Figure 4 shows the integrated I_2^+ signal as a function of time delay. The ionization rate peaks at about 330 fs, corresponding to $R_c = 8.5$ a.u., which agrees well with our previous results [7]. In this case, there is no dissociation, so the signal is the same as what we measured before and corresponds to enhanced ionization of the orbital associated with the B state of the neutral molecule. A secondary peak at 1250 fs comes from the wave packet returning to R_c. However, this shows the difficulty of tracking the wave packet at later times, due to the severe dispersion. $\langle R \rangle$ never reaches R_c after the initial time. In addition, the wave packet becomes very wide. Despite, this, we see a clear secondary peak, and

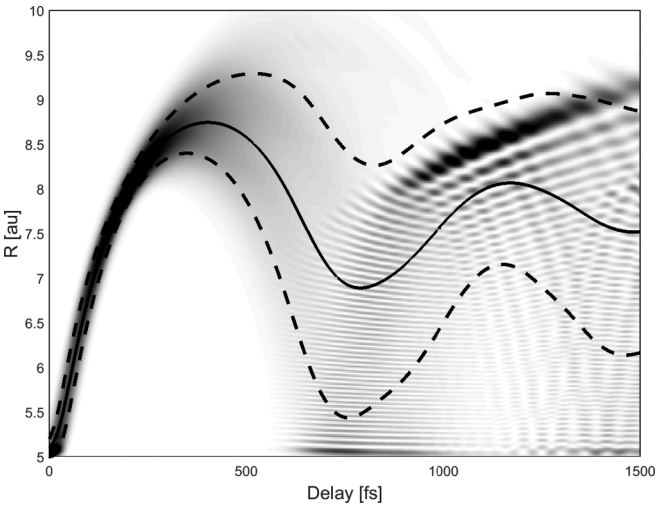

FIG. 2. Full wave packet following excitation from the X to B state at 513 nm. Solid line corresponds to $\langle R \rangle$; dashed lines correspond to the rms width of the wave packet.

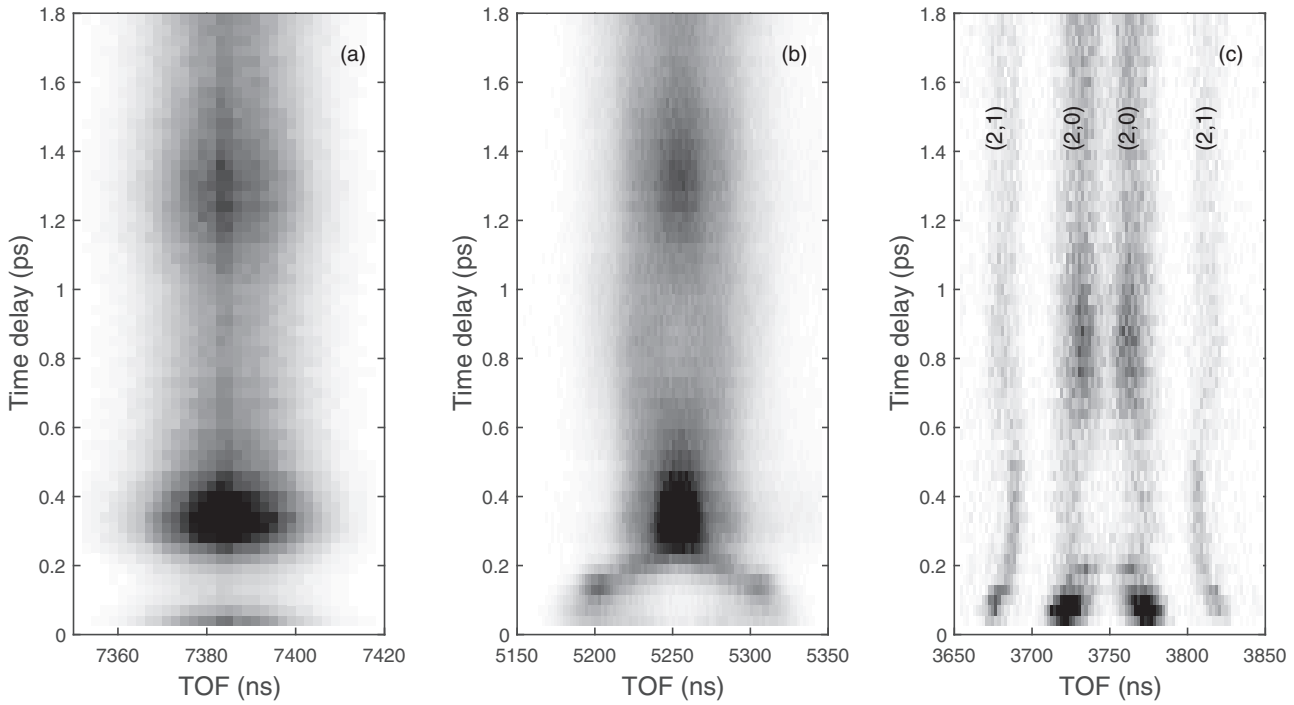

FIG. 3. TOF spectrum as a function of time delay for different ionization channels. (a) I_2^+: while there is no dissociation, the molecular ion does have a distribution of thermal energies, producing a distribution of TOFs; (b) I^+: this TOF range includes the $I^+ + I$ dissociation channel. Zero KER corresponds to 5250 ns, and the KER can lead to shorter or longer TOF depending on whether the I^+ ion is initially directed along the TOF axis towards or away from the detector. There can also be a contribution from zero KER I_2^{2+}; and (c) I^{2+}: similarly, this TOF range includes $I^{2+} + I$, corresponding to the central two tracks, and $I^{2+} + I^+$, corresponding to the outer two tracks.

Fig. 2 explains why. There is an interesting focusing effect that occurs in the wave packet between 1000 and 1400 fs. This is a general phenomenon seen in wave packets moving in highly dispersive potentials and can be associated with caustic lines in the classical trajectories [18]. Although the wave packet is spread over a large range in R, there is a pronounced ridge extending from $R = 8$ to 9 a.u. Since this ridge passes through R_c at around 1250 fs, it produces the secondary peak in the I_2^+ signal. Thus, despite the strong dispersion, it is possible to interpret the results at large time delays and will confirm an identification made below.

The first new result comes from analyzing the I^+ signal. Previously we did not energy resolve this signal because, at the time, we did not understand the origin of the (1,0)

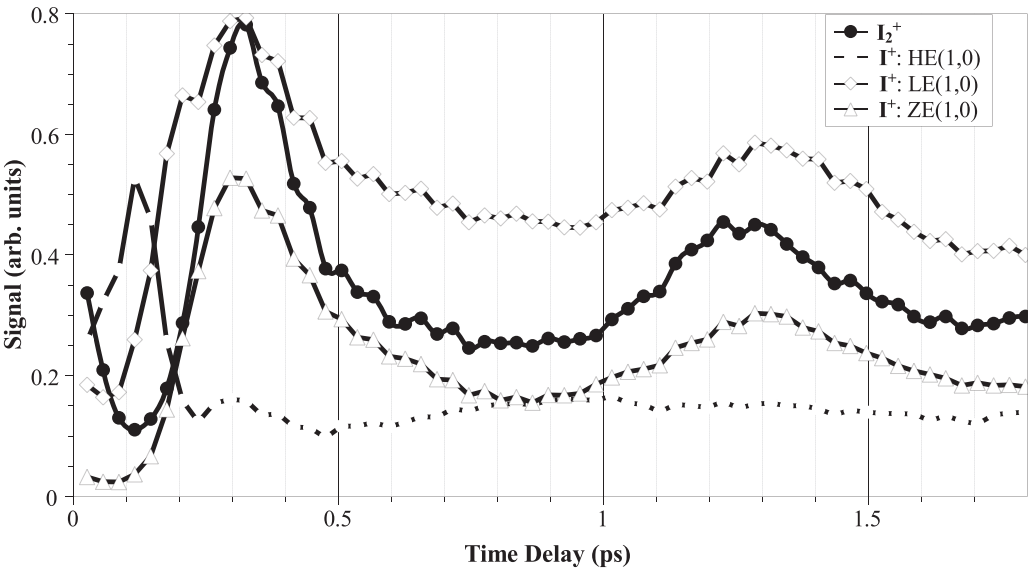

FIG. 4. Integrated signals for I_2^+, zero, low, and high energy I^+.

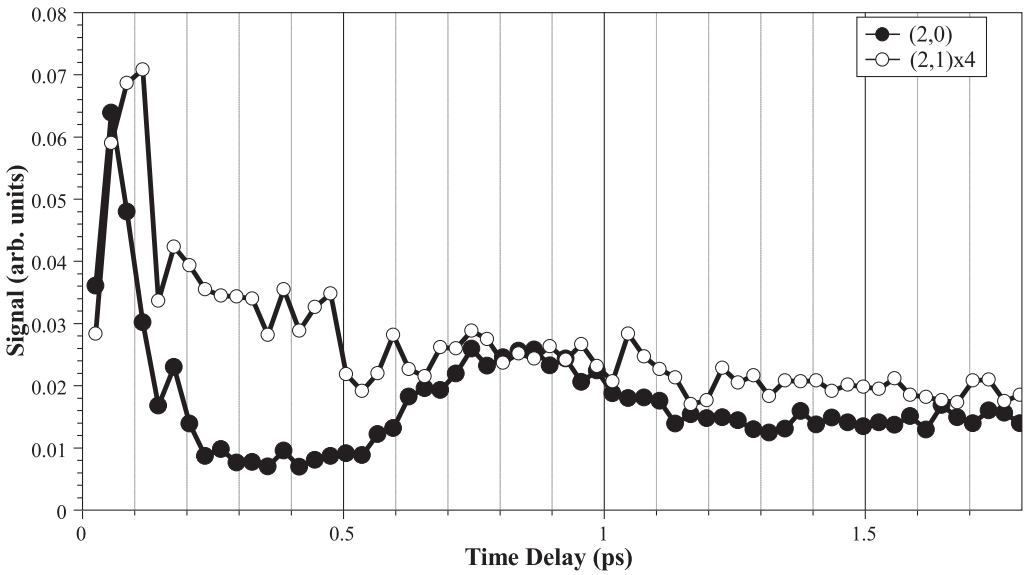

FIG. 5. Integrated signal for the (2,0) and (2,1) dissociation channels.

dissociation channel. In fact, this is what led to the experiments reported in Refs. [14,15], as we wanted to delve into origins of the (1,0) signal. We now understand that the low-energy signal LE(1,0) comes from outer-orbital ionization and the high-energy signal HE(1,0) comes from inner-orbital ionization. In addition to the I_2^+ signal, Fig. 4 shows three signals coming from the I^+ data: HE(1,0), LE(1,0), and ZE(1,0). The latter is the component of the signal with no KER. Specifically, ZE(1,0) includes energies from 0 to 0.023 eV, LE(1,0) includes 0.035 to 0.21 eV, and HE(1,0) includes 0.24 to 3.43 eV. [16] For single-pulse ionization, i.e., ionization that occurs at the equilibrium internuclear separation R_e, the zero KER peak is attributed to the dication, I_2^{2+}. This is because I_2^{2+} is metastable and will have no KER. But it is metastable only near R_{eq}, otherwise it will dissociate into $I^+ + I^+$. So, as the molecule expands on the B state potential energy curve, I_2^{2+} cannot be formed past roughly 6 au. and the ZE(1,0) signal must come from very low-energy $I^+ + I$ dissociation and will be discussed below.

The HE(1,0) signal shows a sharp increase in ionization rate around 100 fs but nowhere else. This peak was seen previously in the integrated (1,0) data [7]. The previous data showed a peak at both 100 and 300 fs, but now we can see that this was a consequence of integrating all of the (1,0) signal. Again, our more recent studies on the details of the (1,0) dissociation channel give more insight into what is going on [15]. The high-energy channel has now been identified with IOI and the lower-energy channel with OOI. While we speculated that there was a mixture of orbitals in the B state, in Ref. [7], we now see that this is not necessary. The two peaks result from ionization from distinct orbitals. Moreover, this is consistent with our speculation that the peak corresponding to smaller R comes from an orbital with a large ionization potential, as will be the case for inner orbitals. Since enhanced ionization comes only from σ orbitals, this means that it must come from at least the HOMO-2. However, this state is associated with ionization to the B state of I_2^+, which dissociates with very little kinetic energy (<0.2 eV). Thus, the high-energy (1,0) must come from the HOMO-3 or HOMO-4, both σ states, as originally suggested. Finally, it is also clear why this signal never comes back at large time delay. Here 100 fs corresponds to about $R = 6.8$ a.u. $\langle R \rangle$ does barely reach this value upon return, the wave function is very spread out, and there is no focusing effect to enhance the signal as there is at 1250 fs around 8.5 a.u.. The detailed origin of the lower energy (1,0) channel is not so clear. It follows the I_2^+ signal, although it is significantly broader. This suggests that ionization of the LUMO may project the molecular ion onto the low-lying X, A, and B states of the ion, as the X and A states result in I_2^+ and the B state produces low-energy (1,0) dissociation.

Double and triple ionization show equally interesting behavior. Returning to the I_2^{2+} signal, the first electron removed will likely be from the LUMO as for the I_2^+ and will show the same R_c. The second electron must also come from an outer antibonding orbital, as the dication is only metastable, and any excess energy would lead to immediate dissociation. These outer orbitals are π orbitals and will not show any critical behavior as a function of R [14], and, thus, I_2^{2+} will closely track the I_2^+ signal. Ground-state I_2^{2+} ions that do dissociate will end up in the charge symmetric (1,1) channel. In fact, the (1,1) does not show any critical behavior. Of all the ionization channels, this one is a puzzle, as it is, again, likely that the first step would be ionization of the LUMO and would show enhanced ionization.

The charge asymmetric (2,0) dissociation channel, shown in Fig. 5, comes from states with enough excitation energy to reach this high-energy dissociation limit. This cannot arise from ionization from the outer orbitals. So, again, we are looking at ionization from the HOMO-3 or HOMO-4 σ orbitals. In addition, we require σ orbitals for enhanced ionization to explain the sharp peak at 50 fs corresponding to $R = 5.8$ a.u. While not as pronounced in Fig. 5, Fig. 3 also shows a clear secondary peak at about 175 fs corresponding to $R = 7.8$ a.u.. Finally, there is a rebound at 800 fs. As the wave packet never strongly returns to 5.8 a.u., the rebound must come from the secondary peak. Figure 2 shows that at $R = 7.8$ a.u.

and a delay of 800 fs, the wave packet starts to focus. This corroborates existence of a secondary peak at 7.8 a.u.

Finally, the triple ionization channel leading to (2,1) dissociation also shows enhanced ionization at 100 fs or $R = 6.8$ au, just like the HE(1,0) channel. For the latter channel, we argued above that there would be no rebound, as the wave packet does not strongly return to 6.8 a.u. Thus, we would predict that the (2,1) will not show a rebound, and this is indeed the case. Tracking the orbitals through three ionization steps is probably pushing the idea of ionization from particular orbitals a bit too far. Each ionization event is going to change the orbital structure and will lead to mixing of states. Nevertheless, it is interesting that the (2,1) channel does have enhanced ionization and that it tracks the high-energy (1,0) channel more than the I_2^+ channel. At the intensities used, it may be that the only way to produce a significant amount of triple ionization is to go through the IOI step that has the highest branching ratio, namely, the high-energy (1,0) channel. This is similar to conclusions we made previously in Ref. [19], where we found that ionization pathways do not always follow the simplest one-electron ionization steps. Rather, various ionization channels often come from previous channels that involved electronic excitation. For example, we found that the $I^{3+} + I^{2+}$ channel was preceded by $I^{3+} + I^{1+}$, rather than $I^{2+} + I^{2+}$.

IV. DISCUSSION

The results presented here agree with the conclusions from our early work, but we now include energy resolution and analyses of channels arising from multiple ionization. The I_2^+ signal is the same as previously observed, showing a clear R_c at 8.5 a.u. We now show that the double peak in the (1,0) channel actually corresponds to two different KERs, and, from our more recent work, we know that this comes from two different orbitals and not from a state of mixed orbitals. These results and the multiple ionization channels can all consistently be explained through one, well-established, organizing principle: enhanced ionization from a double-well potential produces a peak in the ionization rate at a particular R for σ orbitals, but not π orbitals. All of the specific channels discussed below are summarized in Table I.

Refering back to Eq. (1), excitation to the B state corresponds roughly to promoting an electron from the $6\pi_g$ orbital to the $11\sigma_u$, although the B state is likely an admixture of several orbitals. In any case, this orbital is responsible for R_c seen in the I_2^+ and the LE(1,0) channels leading to population in the X, A, and/or B states of the ion. The X and A states of the ion do not dissociate and are detected as I_2^+, while the B state dissociates with low KER. In fact, the B state of the ion is quite flat and at larger R, will dissociate with virtually no KER, leading to the apparent zero KER (1,0) signal, which could be mistaken for I_2^{2+}. Thus, I_2^+, LE(1,0), and ZE(1,0) all come from enhanced ionization of the $11\sigma_g$ orbital and have the same R dependence.

TABLE I. Connections between moelcular orbitals and ionization channels

Channel	Orbital	Time delay (fs)	R (a.u.)	Rebound (fs)
I_2^+	LUMO	330	8.5	1250
LE(1,0)	LUMO/HOMO	330	8.5	1300
HE(1,0)	HOMO-3, -4	100	6.8	None
(1,1)	HOMO/HOMO-1	N/A	N/A	N/A
HE(2,0)	HOMO-3, -4	50	5.8	None
LE(2,0)	HOMO-3, -4	175	7.8	800
(2,1)	HOMO-3, -4	100	6.8	None

The HE(1,0) signal has only one peak and appears not to be a mixture of orbitals, as, at that R, there is no LE(1,0) signal. The HOMO-2 only leads to low-energy KER, but the HOMO-3 and -4 have been associated with high-energy KER. Moreover, the HOMO-3 and -4 are σ orbitals and will go through enhanced ionization at some R. It is predicted that deeper binding leads to a smaller R_c, which is again consistent with our observations. We previously saw HE(1,0) dissociation in a single-pulse wavelength study. At a particular wavelength, we saw almost 100% branching to the HE(1,0) state. This wavelength was close to the X to B resonance. In the present work, we are probing at 800 nm, which is far from the wavelength at which we saw the HE(1,0). While at R_e, 800 nm is not resonant with the X to B transition, at larger R (longer delays) the X to B transition energy becomes smaller. The exact R where the HE(1,0) peak appears does not occur when the X to B transition is in resonance with 800 nm. However, the exact mechanism for coupling to inner orbitals to cause ionization is not yet understood. Nevertheless, in both studies, the IOO occurs when the transition is slightly less than the frequency of the laser light.

In both studies, fixed R, variable wavelength, and fixed wavelength, variable R, we find critical points where the ionization rate and coupling to inner orbitals is enhanced. Thus, there must be a deeper unifying principle. A complete experiment would be to do both: launch a wave packet on the B state of the neutral and probe as a function of time and wavelength to fully map out the strong-field interaction.

V. CONCLUSIONS

By studying strong-field ionization of iodine as a function of R, at fixed wavelength, we find that many orbitals play a role in the strong-field interaction, even if the orbitals are deeply bound (i.e., more bound than the HOMO by at least several photon energies). In addition, the coupling appears to select the σ orbitals, which are known to have a critical internuclear separation, although previously this was considered only for the highest orbital. We now find critical points for all the populated orbitals, even deeply bound ones. Both R_c and one-photon resonances appear to cause the strong coupling to the inner orbitals.

ACKNOWLEDGMENT

We would like to acknowledge support from the NSF under Grant No. NSF-PHYS-1707542.

[1] T. Seideman, M. Yu. Ivanov, and P. B. Corkum, Role of Electron Localization in Intense-Field Molecular Ionization, Phys. Rev. Lett. **75**, 2819 (1995).

[2] T. Zuo and A. D. Bandrauk, Charge-resonance-enhanced ionization of diatomic molecular ions by intense lasers, Phys. Rev. A **52**, 2511(R) (1995).

[3] Th. Ergler, B. Feuerstein, A. Rudenko, K. Zrost, C. D. Schröter, R. Moshammer, and J. Ullrich, Quantum-Phase Resolved Mapping of Ground-State Vibrational D_2 Wave Packets Via Selective Depletion in Intense Laser Pulses, Phys. Rev. Lett. **97**, 103004 (2006).

[4] L. Fang and G. N. Gibson, Strong-Field Induced Vibrational Coherence in the Ground Electronic State of Hot I_2, Phys. Rev. Lett. **100**, 103003 (2008).

[5] J. P. Nibarger, M. Li, S. Menon, and G. N. Gibson, Direct Observation of Excited State Fragments Following Molecular Ionization and Dissociation in Strong Fields, Phys. Rev. Lett. **83**, 4975 (1999).

[6] R. N. Coffee and G. N. Gibson, VUV fluorescence from selective high order multiphoton excitation of N_2, Phys. Rev. A **69**, 053407 (2004).

[7] H. Chen, V. Tagliamonti, and G. N. Gibson, Enhanced ionization of an inner orbital of I_2 by strong laser fields, Phys. Rev. A **86**, 051403(R) (2012).

[8] B. K. McFarland, J. P. Farrell, P. H. Bucksbaum, and M. Gühr, High harmonic generation from multiple orbitals in N_2, Science **322**, 1232 (2008).

[9] J. Itatani, J. Levesque, D. Zeidler, H. Niikura, H. Pépin, J. C. Kieffer, P. B. Corkum, and D. M. Villeneuve, Tomographic imaging of molecular orbitals, Nature (London) **432**, 867 (2004)

[10] M. V. Ammosov, N. B. Delone, and V. P. Krainov, Tunnel ionization of complex atoms and of atomic ions in an alternating electromagnetic field, Zh. Eksp. Teor. Fiz. **91**, 2008 (1986) [Sov. Phys. JETP **64**, 1191 (1986)].

[11] M. P. de Boer and H. G. Muller, Observation of Large Populations in Excited States After Short-Pulse Multiphoton Ionization, Phys. Rev. Lett. **68**, 2747 (1992).

[12] T. Nubbemeyer, K. Gorling, A. Saenz, U. Eichmann, and W. Sandner, Strong-Field Tunneling without Ionization, Phys. Rev. Lett. **101**, 233001 (2008).

[13] G. Gibson, T. S. Luk, A. McPherson, K. Boyer, and C. K. Rhodes, Observation of a new inner-orbital molecular transition at 55.8 nm in N_2^{2+} produced by multiphoton coupling, Phys. Rev. A **40**, 2378 (1989).

[14] G. Lagmago Kamta and A. D. Bandrauk, Effects of molecular symmetry on enhanced ionization by intense laser pulses, Phys. Rev. A **75**, 041401(R) (2007).

[15] D. L. Smith, V. Tagliamonti, J. Dragan, and G. N. Gibson, Single ionization of molecular iodine, Phys. Rev. A **95**, 013410 (2017).

[16] D. L. Smith and G. N. Gibson, Resonantly enhanced inner orbital ionization in molecular iodine, Phys. Rev. A **97**, 021401(R) (2018).

[17] W. A. de Jong, L. Visscher, and W. C. Nieuwpoort, Relativistic and correlated calculations on the ground, excited, and ionized states of iodine, J. Chem. Phys. **107**, 9046 (1997).

[18] V. A. Ermoshin, V. Engel, and C. Meier, Oscillatory pump–probe signals from delocalized wave packets, J. Chem. Phys. **113**, 5770 (2000).

[19] S. V. Menon, J. P. Nibarger and G. N. Gibson, A framework for understanding molecular ionization in strong laser fields, J. Phys. B **35**, 2961 (2002).